Pre-print submitted version

Radiative and non-Radiative Losses Analysis by In-situ Photoluminescence in Perovskite Solar Cell Current-Voltage Curves

Chris Dreessen,[1] Daniel Pérez-del-Rey,[1] Pablo P. Boix,[2*] Henk J. Bolink[1]

[1] Instituto de Ciencia Molecular, Universitat de València, c. J. Beltran 2, Paterna, Spain

[2] Institut de Ciència dels Materials, Universitat de València, c. J. Beltran 2, Paterna, Spain

* Corresponding author: pablo.p.boix@uv.es

Abstract

The rapid development of perovskite solar cells has been based on improvements in materials and device architectures, yet further progress towards their theoretical limit will require a detailed study of the main physical processes determining the photovoltaic performance. Luminescence can be a key parameter for this purpose, as it directly assesses radiative recombination. We present steady-state absolute photoluminescence of an operating device at varying voltages as a tool to study the loss mechanisms in perovskite devices. The technique gives access to the variation of the relative radiative /non-radiative recombination weighted along the measured potentials, and allows identifying charge extraction deficits at short-circuit conditions, which we show on a vacuum-deposited solar cell. These measurements can be crucial to characterize the nature of the charge losses, a step to develop approaches to improve this photovoltaic technology.

1. Introduction

Since the first report on metal halide perovskites for solar cells applications[1] to their current efficiency record of 25.2%,[2] this technology has experienced an unprecedented evolution in the photovoltaic field.[3,4] The power conversion efficiency (*PCE*) is often discussed in terms of short-circuit current (J_{SC}), open-circuit potential (V_{OC}) and fill factor (*FF*). These are obtained at different voltages, so the comparison with their respective theoretical maximum values, established by the Shockley-Queisser limit,[5] provides substantial insights about the main limitations of the device performance. For instance, at open-circuit conditions (OC) no charge is extracted, meaning that the absorbed charges will recombine either radiatively or non-radiatively. Therefore, V_{OC} below the ideal one can be indicative of non-radiative recombination (in the case that the quasi-Fermi level splitting (QFLS) is not limited by the contacts). At short-circuit conditions (SC, V = 0V) it is usually assumed that all photogenerated charges are extracted. Consequently, a low J_{SC} in halide perovskite solar cell is commonly attributed to a deficit in charge carrier generation, which can be caused by low perovskite absorbance or by light management problems (such as reflection or parasitic absorption of the transport layers). Nevertheless, if there are extraction problems (e.g. due to charge barriers or low mobility), charges might recombine even at SC and thus reduce J_{SC}. The *FF* is ideally determined by the V_{OC} and the ideality factor, and therefore recombination-dependent, but transport problems (due to series and shunt resistances) can further reduce its value.[6]

All these three parameters are approaching their theoretical radiative limit in metal halide perovskite solar cells.[7] To identify the remaining shortcomings of perovskite solar cells it is necessary to obtain a thorough understanding on the cells working mechanisms. However, it is not straight forward to identify the physical processes limiting the device performance of metal halide perovskite solar cells. Their unusual properties, such as ion migration, complicate the grasp of these devices.[8,9]

In this context, the photoluminescence (PL) response can be a useful tool to gain insight into the remaining losses. Often, the PL signal of different perovskite films is qualitatively compared to point out the film quality variations,[10–12] where a higher PL signal is ascribed to lower non-radiative recombination. Moreover, if PL is measured in an absolute scale, the signal can be related to the QFLS in the absorber layer of the device.[13] Examples of this comprise perovskite solar cells studies about the QFLS differences in different compositions,[14] surface passivation evaluation,[15] interface voltage losses,[16] spatial homogeneity of the QFLS,[17] and ideality factor[18] among others. All these measurements were performed at OC conditions (not contacted) where the PL intensity

should be maximal since all the generated charge carriers need to recombine. On the other hand, full devices can be contacted and set under different bias conditions during the PL measurement. At SC, the PL should vanish in an ideal solar cell as all the charge carriers should be extracted. This can be used to distinguish between absorption and extraction problems at SC.[19,20]

Here, we propose the use of bias-dependent absolute PL to estimate non-radiative to radiative recombination rates along the current-voltage (JV) curve measured at one sun equivalent. The technique can identify the radiative losses at SC, as well as the ratio between radiative and non-radiative recombination at different voltage potentials, which provides a useful tool to study the origin of the losses in halide perovskite solar cells.

2. Results and Discussion

2.1 Theory

To obtain information about the recombination rates one has to study the detailed balance between charge generation and charge recombination/extraction. We define J_{gen} as the current density of free charge carriers photogenerated within the absorber (and express it therefore in units of electrical current density, mA/cm^2), where we integrate the charge carrier generation rate, *G,* over the absorber thickness. Considering the low exciton binding energy of $CH_3NH_3PbI_3$ (MAPI),[21] this value can be assumed voltage-independent. The maximum value for J_{gen} (defined as J_{max}) can be found by assuming that all photons in the solar spectrum (AM1.5G, one sun) above the perovskite bandgap (E_g) are absorbed and generate and electron-hole pair. For our vacuum-deposited MAPI in the cubic phase,[22] with a typical E_g = 1.61eV one finds J_{max} = 25.1mA/cm^2 (see Figure 1, violet line).[23] The actual value of J_{gen} (see Figure 1, blue line) is reduced mainly by reflection and parasitic absorption. The generated charge carriers can be extracted in form of current density, $J_{extracted}$ (Figure 1, red dots and green line) or they recombine (Figure 1, yellow area), either radiatively (associated to a radiative recombination current J_{rad}) or non-radiatively (associated to a non-radiative recombination current $J_{non\text{-}rad}$). These three processes are in general voltage dependent. Therefore,

$$\begin{aligned} J_{\mathrm{gen}} &= J_{\mathrm{extracted}}(V) + J_{\mathrm{recomb}}(V) \\ &= J_{\mathrm{extracted}}(V) + J_{\mathrm{rad}}(V) + J_{\mathrm{non-rad}}(V). \end{aligned} \quad (1)$$

At OC conditions, there is no net current flow from the device contacts ($J_{extracted}(V_{OC}) = 0$), so J_{gen} and the recombination rates compensate:

$$J_{gen} = J_{rad}(V_{OC}) + J_{non-rad}(V_{OC}). \quad (2)$$

Ideally, all the charge carriers are extracted at SC conditions ($J_{gen} = J_{SC}$), a situation which is generally assumed. However, in a real device, it can happen that the charge extraction is not substantially faster than the recombination and therefore also the radiative and non-radiative current densities should be taken into account.

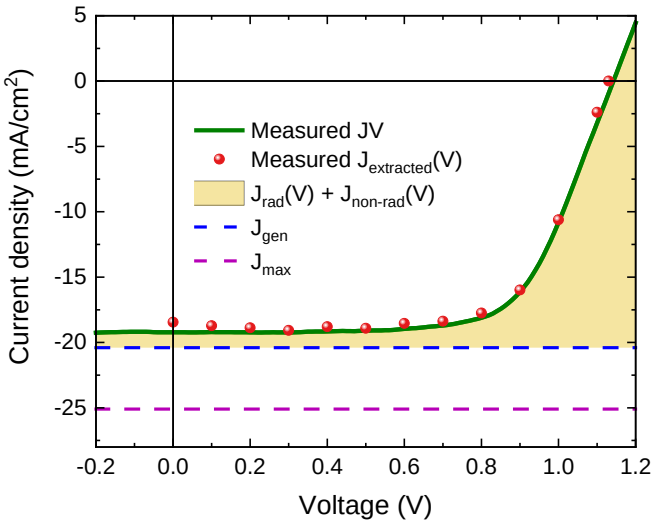

Figure 1. JV characteristics under one sun equivalent of the analyzed solar cell. The dots represent the current density measured concurrently with the steady-state absolute PL ($J_{extracted}$) while the green line shows a JV scan at this illumination with a scan speed of about 0.3V/s. The recombinative losses are shaded in yellow.The blue dashed line is an estimation of the total photogenerated current in the device (J_{gen}) assuming voltage-independent charge generation, and the purple dashed line (J_{max}) represents its maximum theoretical value.

Typically, only $J_{extracted}(V)$ is reported for solar cells. By placing an integrating sphere which is calibrated to absolute photon numbers onto the electrically contacted solar cell, it is possible to record $J_{extracted}(V)$ and $J_{rad}(V)$ simultaneously (for more details see supporting information). Here, we neglect other minor possible losses such as light which is laterally guided out of the structure or absorbed by the transport layers and thus not collected. In spite of the additional knowledge of J_{rad}, both J_{gen} and $J_{non-rad}(V)$ remain elusive. Although $J_{non-rad}(V_{OC})$ can in principle be measured via the PL quantum yield (PLQY), we do not use it here for two reasons: from the practical point

of view, it is too low in the measured sample, so that the measurement uncertainty inhibits the exact calculation of $J_{\text{non-rad}}(V)$. On the other hand, PLQY usually includes parasitic absorption within the non-radiative recombination, which we would like to try to separate. Nonetheless, even without further measurements, one can make use of the voltage-independent nature of J_{gen} to extract information about the ratio of $J_{\text{rad}}(V)$ and $J_{\text{non-rad}}(V)$ by relating two measurements at different bias voltages:

$$\frac{\Delta J_{\text{rad}}}{\Delta J_{\text{non-rad}}} \equiv \frac{J_{\text{rad}}(V_1) - J_{\text{rad}}(V_2)}{J_{\text{non-rad}}(V_1) - J_{\text{non-rad}}(V_2)} = \frac{-1}{\frac{J_{\text{extracted}}(V_1) - J_{\text{exctracted}}(V_2)}{J_{\text{rad}}(V_1) - J_{\text{rad}}(V_2)} + 1} \qquad (3)$$

This can be interpreted as the slope of a $J_{\text{rad}}(V)$ vs. $J_{\text{non-rad}}(V)$ curve. We point out that this is not a proper function and therefore the quantity $\Delta J_{\text{rad}}/\Delta J_{\text{non-rad}}$ needs to be treated with care. However, if this "slope" is constant one can deduce that the ratio of $J_{\text{rad}}/J_{\text{non-rad}}$ is constant over the voltage range. If the "slope" changes the ratio changes as well, which can give important information about the non-radiative recombination source.

2.2 Experimental Results

All measurements are performed on an inverted vacuum-deposited MAPI solar cell similar to those reported elsewhere[24,25], with an architecture consisting of an indium tin oxide (ITO) coated glass slide, covered with molybdenum (VI) oxide (MoO_3, 5nm) / *N*4,*N*4,*N*4″,*N*4″-tetra([1,1′-biphenyl]-4-yl)-[1,1′:4′,1″-terphenyl]-4,4″-diamine (TaTm, 10nm) / MAPI (590nm) / fullerene (C_{60}, 25nm) / bathocuproine (BCP, 7nm) / silver (Ag, 100nm). The JV measurement under simulated AM1.5G illumination results in V_{OC} = 1.11V, *FF* = 70%, and J_{SC} = 18.0mA/cm^2, yielding *PCE* = 14.0% (see Figure S3).

The setup for simultaneous measurement of $J_{\text{extracted}}(V)$ and $J_{\text{rad}}(V)$ consists of an electrical holder for the masked solar cell with an integrating sphere on top. The solar cell is illuminated by a green laser (λ = 522nm) under one sun equivalent which is achieved by matching the J_{SC} obtained by the measurement using the solar simulator. The solar cell JV measured under this illumination achieves a V_{OC} = 1.13V, *FF* = 68%, and J_{SC} = 19.2mA/cm^2 (Figure 1); values which are comparable to the ones measured under AM1.5G one sun simulated illumination. The PL signal is separated from the laser via a 600nm long-pass filter and collected in a spectrometer. For further details about the experimental methods see the supporting information.

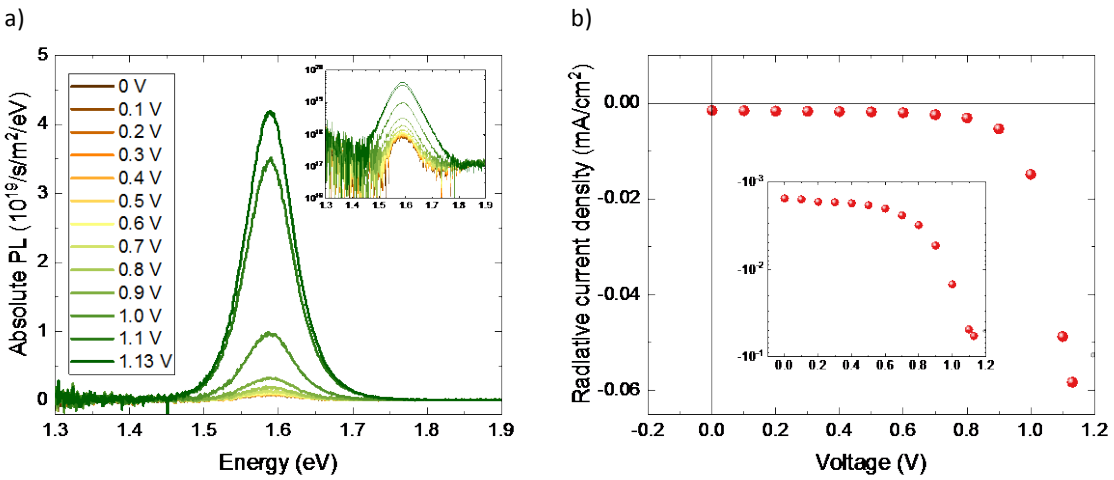

Figure 2. Absolute photoluminescence spectra obtained at different steady state operating voltages for the solar cell measured under one sun equivalent in the forward direction (a) and J_{rad} derived from them (b).

The measurement and integration of the steady-state absolute PL at bias potentials along the JV curve enables the direct estimation of J_{rad} (see Figure 2) by integrating the PL peak and multiplying the integral with the electric charge of an electron. In order to check the validity of this measurement, the QFLS was calculated from the luminescence via the fit of the high-energy tail following previously reported procedures,[26] obtaining a value of 1.13 eV in excellent agreement with the electrically measured V_{OC} (details in the supporting information).

The emission has to be maximum at OC conditions, where there is no net current flow ($J_{extracted}$ = 0). In the ideal case, non-radiative recombination paths are considered inactive and thus $J_{non\text{-}rad}$ = 0 and $J_{gen} = J_{rad}$. The fact that $J_{SC} \leq J_{gen} \leq J_{max}$ and that the radiative current is orders of magnitude below J_{SC} (compare Figures 1 and 2) indicates the existence of significant non-radiative losses.

At SC conditions, full extraction is often assumed, implying thus that $J_{gen} = J_{SC}$, in which case no recombination should happen and no light should be emitted from the solar cell.[20] Despite the recorded luminescence at V=0 is small (Figure 2), its value different from zero implies radiative losses compared to the ideal fully-quenched case. This kind of signal at SC conditions would be expected in the case of low mobility systems[19] or other charge extraction limitations, circumstance which has also been discussed for metal halide perovskites.[27] Assuming that the relation $J_{non\text{-}rad} >> J_{rad}$ is also fulfilled at SC, as discussed below, $J_{non\text{-}rad}$ might not be negligible and therefore $J_{gen} > J_{SC}$, as previously suggested by other electrical techniques.[28]

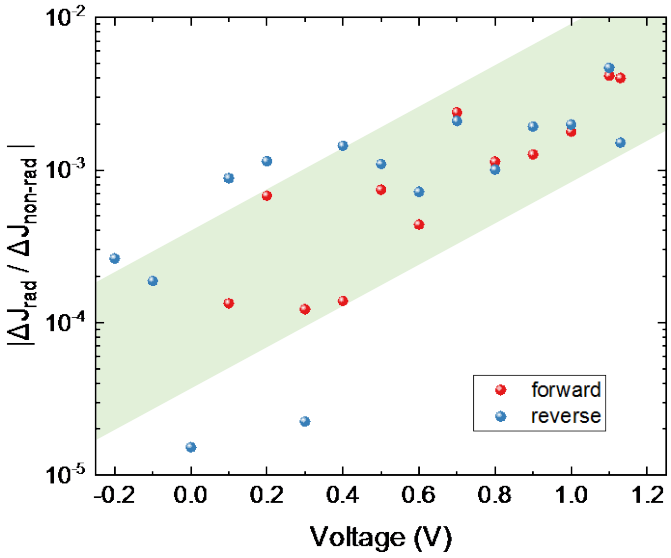

Figure 3 Ratio between the evolution of radiative and non-radiative losses of the solar cell under one sun equivalent measured at different voltages. Both forward and reverse scans are represented.

To find out more about $J_{non\text{-}rad}$ we evaluate the ratio between radiative and non-radiative recombination at different bias voltages. Using Equation 3 we can obtain this information without further approximations. Figure 3 shows the ratio $\Delta J_{rad}/\Delta J_{non\text{-}rad}$ for both the forward and the reverse scan directions. In the end of the reverse scan, the cell started to degrade, making the data points at low voltages (V < 0.5V) less trustworthy. Interestingly, the ratio of the differences in radiative and non-radiative current is not constant with the voltage, implying that also the ratio of radiative and non-radiative recombination depends on the voltage. Since $\Delta J_{rad}/\Delta J_{non\text{-}rad}$ is increasing with V, it follows that at SC there is relatively more non-radiative loses than at OC, with respect to the radiative recombination. At all voltages $\Delta J_{rad}/\Delta J_{non\text{-}rad} < 1$ due to smaller changes in the radiative current than in the non-radiative current, which is expected for $J_{non\text{-}rad} >> J_{rad}$.

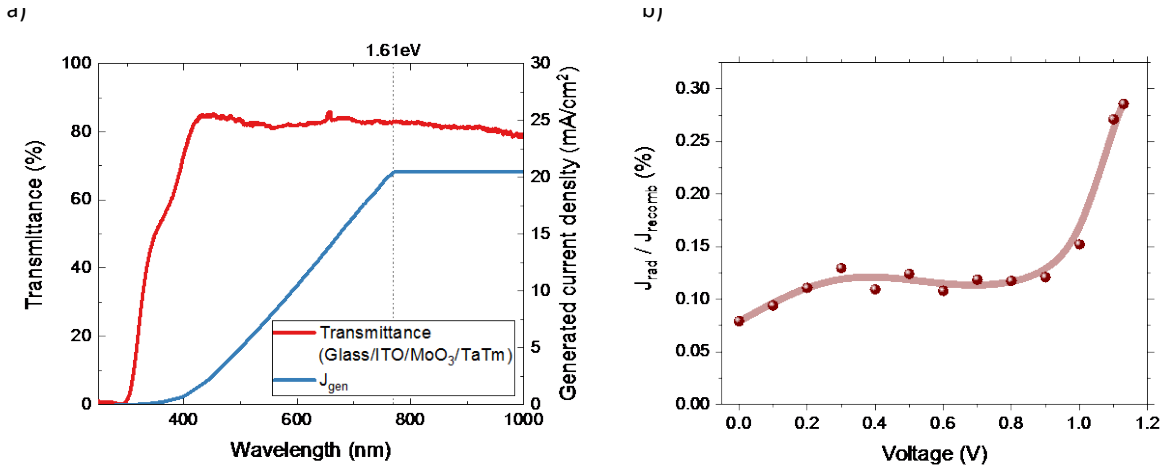

Figure 4. a) Transmittance of glass, ITO, hole transporting and selective materials of the device accounting for the optical losses in the full device (red line). This values are considered in the J_{gen} calculation (blue line). b) Absolute ratio between radiative recombination losses and total recombination losses in the solar cell dependent on the voltage bias.

In an attempt to quantify $J_{non\text{-}rad}$ we estimate J_{gen} from the transmittance data of the layers on top of the perovskite (glass/ITO/MoO_3/TaTm, see Figure 4a), which includes the reflection and parasitic absorption of these layers. We furthermore measured the reflection of the full device and show that it is mainly determined by the reflection of the glass slide (see Figure S5). This approach neglects the parasitic absorption of the layers on the bottom, assumed to play just a minor role for light reflected at the metal contact. By multiplying the transmittance with the solar spectrum (AM1.5G) and integrating all the energies above the bandgap, we find that the current of generated charge carriers under 1 sun illumination is J_{gen} = 20.4 mA/cm^2. As in the entire work, we assume that the recombination currents depend on the charge carrier densities rather than on the light source, and therefore J_{gen} is equal for the laser excitation and the excitation by the solar simulator. Considering these approximations, around 2 mA/cm^2 are lost due to recombination at SC conditions (J_{recomb}) and $J_{gen} \neq J_{SC}$. As discussed above, these losses are mainly attributed to non-radiative recombination, yet they have a contribution from the radiative one.

The evolution of the ratio of radiative recombination and total losses as a function of the voltage is presented in Figure 4b, which confirms that non-radiative recombination is the dominant process along the entire JV curve, although its weight is reduced towards OC. This indicates that the non-radiative recombination mechanisms change depending on the bias voltage, an

observation which may help to identify their nature. Further investigations to find the source of this change can be a valuable tool to reduce the photovoltaic losses in the devices.

We want to point out that this study of absolute radiative and non-radiative currents is sensitive towards many factors. Here, we do not consider parasitic absorption and outcoupling losses of the emitted light, which may lead to an underestimation of J_{rad}. However, we do not expect that these mechanisms are voltage dependent, and therefore our approximation preserve the result that non-radiative recombination is relatively increased towards SC conditions.

3. Conclusions

The measurement of the steady-state absolute photoluminescence of an operating perovskite solar cell enables the study of the loss mechanisms in the device. The radiative recombination, extracted from the integration of the radiative emission, is maximum at OC as expected, yet it is not totally quenched at SC. This suggests non-ideal charge extraction problems, which opens a device configuration improvement pathway. Finally, based on an estimation of the total photogenerated charge, we present the relative variation of radiative and non-radiative losses along the JV curve, which can be useful to identify the sources of the main losses. This work presents a tool to study the origin of the losses in perovskite solar cells, a necessary step to pursue the way towards the theoretical performance limit of this technology.

Acknowledgment

This work has been partially supported by Generalitat Valenciana (SEJI2017/2017/012), Ministerio de Economía y Competitividad of Spain (MAT2017-88905-P and MAT2017-88821-R). PPB would like to thank Ministerio de Economía y Competitividad of Spain for his RyC contract.

References

(1) Kojima, A.; Teshima, K.; Shirai, Y.; Miyasaka, T. Organometal Halide Perovskites as Visible-Light Sensitizers for Photovoltaic Cells. *J. Am. Chem. Soc.* **2009**, *131* (17), 6050–6051. https://doi.org/10.1021/ja809598r.

(2) National Renewable Energy Laboratory, NREL. PV Research Cell Record Efficiency Chart.

(3) Jena, A. K.; Kulkarni, A.; Miyasaka, T. Halide Perovskite Photovoltaics: Background, Status, and Future Prospects. *Chem. Rev.* **2019**, *119* (5), 3036–3103. https://doi.org/10.1021/acs.chemrev.8b00539.

(4) A Decade of Perovskite Photovoltaics. *Nat. Energy* **2019**, *4* (1), 1–1.

https://doi.org/10.1038/s41560-018-0323-9.

(5) Shockley, W.; Queisser, H. J. Detailed Balance Limit of Efficiency of P-n Junction Solar Cells. *J. Appl. Phys.* **1961**, *32* (3), 510. https://doi.org/10.1063/1.1736034.

(6) Green, M. Accuracy of Analytical Expressions for Solar Cell Fill Factors. **1983**, *7* (1), 337–340.

(7) Tress, W. Perovskite Solar Cells on the Way to Their Radiative Efficiency Limit - Insights Into a Success Story of High Open-Circuit Voltage and Low Recombination. *Adv. Energy Mater.* **2017**, *7* (14), 1602358. https://doi.org/10.1002/aenm.201602358.

(8) Harwell, J. R.; Baikie, T. K.; Baikie, I. D.; Payne, J. L.; Ni, C.; Irvine, J. T. S.; Turnbull, G. A.; Samuel, I. D. W.; Stranks, S. D.; Eperon, G. E.; et al. Probing the Energy Levels of Perovskite Solar Cells via Kelvin Probe and UV Ambient Pressure Photoemission Spectroscopy. *Phys. Chem. Chem. Phys.* **2016**, *342* (29), 341–344. https://doi.org/10.1039/C6CP02446G.

(9) Almora, O.; García-Batlle, M.; Garcia-Belmonte, G. Utilization of Temperature-Sweeping Capacitive Techniques to Evaluate Band Gap Defect Densities in Photovoltaic Perovskites. *J. Phys. Chem. Lett.* **2019**, *10* (13), 3661–3669. https://doi.org/10.1021/acs.jpclett.9b00601.

(10) deQuilettes, D. W.; Vorpahl, S. M.; Stranks, S. D.; Nagaoka, H.; Eperon, G. E.; Ziffer, M. E.; Snaith, H. J.; Ginger, D. S. Impact of Microstructure on Local Carrier Lifetime in Perovskite Solar Cells. *Science (80-.).* **2015**, No. April. https://doi.org/10.1126/science.aaa5333.

(11) Yantara, N.; Bhaumik, S.; Yan, F.; Sabba, D.; Dewi, H. A.; Mathews, N.; Boix, P. P.; Demir, H. V.; Mhaisalkar, S. Inorganic Halide Perovskites for Efficient Light-Emitting Diodes. *J. Phys. Chem. Lett.* **2015**, *6* (21), 4360–4364. https://doi.org/10.1021/acs.jpclett.5b02011.

(12) Jiang, Q.; Zhang, L.; Wang, H.; Yang, X.; Meng, J.; Liu, H.; Yin, Z.; Wu, J.; Zhang, X.; You, J. Enhanced Electron Extraction Using SnO2 for High-Efficiency Planar-Structure HC(NH2)2 PbI3-Based Perovskite Solar Cells. *Nat. Energy* **2017**, *2* (1). https://doi.org/10.1038/nenergy.2016.177.

(13) P.Würfel. The Chemical Potential of Radiation. *J. Phys. C Solid State Phys.* **1982**, *15*, 3967–3985.

(14) Braly, I. L.; Hillhouse, H. W. Optoelectronic Quality and Stability of Hybrid Perovskites from MAPbI3to MAPbI2Br Using Composition Spread Libraries. *J. Phys. Chem. C* **2016**, *120* (2), 893–902. https://doi.org/10.1021/acs.jpcc.5b10728.

(15) Braly, I. L.; DeQuilettes, D. W.; Pazos-Outón, L. M.; Burke, S.; Ziffer, M. E.; Ginger, D. S.; Hillhouse, H. W. Hybrid Perovskite Films Approaching the Radiative Limit with over 90% Photoluminescence Quantum Efficiency. *Nat. Photonics* **2018**, *12* (6), 355–361. https://doi.org/10.1038/s41566-018-0154-z.

(16) Stolterfoht, M.; Wolff, C. M.; Márquez, J. A.; Zhang, S.; Hages, C. J.; Rothhardt, D.; Albrecht, S.; Burn, P. L.; Meredith, P.; Unold, T.; et al. Visualization and Suppression of Interfacial Recombination for High-Efficiency Large-Area Pin Perovskite Solar Cells - Supplementary Information. *Nat. Energy* **2018**. https://doi.org/10.1038/s41560-018-0219-8.

(17) El-Hajje, G.; Momblona, C.; Gil-Escrig, L.; Ávila, J.; Guillemot, T.; Guillemoles, J.-F.; Sessolo, M.; Bolink, H. J.; Lombez, L. Quantification of Spatial Inhomogeneity in Perovskite Solar Cells by Hyperspectral Luminescence Imaging. *Energy Environ. Sci.* **2016**, *9* (7), 2286–2294. https://doi.org/10.1039/C6EE00462H.

(18) Caprioglio, P.; Stolterfoht, M.; Wolff, C. M.; Unold, T.; Rech, B.; Albrecht, S.; Neher, D. On the Relation between the Open-Circuit Voltage and Quasi-Fermi Level Splitting in Efficient Perovskite Solar Cells. *Adv. Energy Mater.* **2019**, *1901631*, 1901631. https://doi.org/10.1002/aenm.201901631.

(19) Rau, U. Reciprocity Relation between Photovoltaic Quantum Efficiency and Electroluminescent Emission of Solar Cells. *Phys. Rev. B* **2007**, *76* (8), 1–8. https://doi.org/10.1103/PhysRevB.76.085303.

(20) Tvingstedt, K.; Malinkiewicz, O.; Baumann, A.; Deibel, C.; Snaith, H. J.; Dyakonov, V.; Bolink, H. J. Radiative Efficiency of Lead Iodide Based Perovskite Solar Cells. *Sci. Rep.* **2014**, *4*, 1–7. https://doi.org/10.1038/srep06071.

(21) D'Innocenzo, V.; Grancini, G.; Alcocer, M. J. P.; Kandada, A. R. S.; Stranks, S. D.; Lee, M. M.; Lanzani, G.; Snaith, H. J.; Petrozza, A. Excitons versus Free Charges in Organo-Lead Tri-Halide Perovskites. *Nat. Commun.* **2014**, *5*, 3586. https://doi.org/10.1038/ncomms4586.

(22) Palazon, F.; Pérez-del-Rey, D.; Dänekamp, B.; Dreessen, C.; Sessolo, M.; Boix, P. P.;

Bolink, H. J. Room-Temperature Cubic Phase Crystallization and High Stability of Vacuum-Deposited Methylammonium Lead Triiodide Thin Films for High-Efficiency Solar Cells. *Adv. Mater.* **2019**, *1902692*, 1902692. https://doi.org/10.1002/adma.201902692.

(23) Rühle, S. Tabulated Values of the Shockley–Queisser Limit for Single Junction Solar Cells. *Sol. Energy* **2016**, *130*, 139–147. https://doi.org/10.1016/j.solener.2016.02.015.

(24) Dänekamp, B.; Droseros, N.; Tsokkou, D.; Brehm, V.; Boix, P. P.; Sessolo, M.; Banerji, N.; Bolink, H. J. Influence of Hole Transport Material Ionization Energy on the Performance of Perovskite Solar Cells. *J. Mater. Chem. C* **2019**, *7* (3), 523–527. https://doi.org/10.1039/C8TC05372C.

(25) Pérez-del-Rey, D.; Gil-Escrig, L.; Zanoni, K. P. S.; Dreessen, C.; Sessolo, M.; Boix, P. P.; Bolink, H. J. Molecular Passivation of MoO3: Band Alignment and Protection of Charge Transport Layers in Vacuum-Deposited Perovskite Solar Cells. *Chem. Mater.* **2019**, acs.chemmater.9b01396. https://doi.org/10.1021/acs.chemmater.9b01396.

(26) Bauer, G. H.; Brüggemann, R.; Tardon, S.; Vignoli, S.; Kniese, R. Quasi-Fermi Level Splitting and Identification of Recombination Losses from Room Temperature Luminescence in Cu(In1-XGax)Se2thin Films versus Optical Band Gap. *Thin Solid Films* **2005**, *480–481*, 410–414. https://doi.org/10.1016/j.tsf.2004.11.061.

(27) Brenner, T. M.; Egger, D. A.; Rappe, A. M.; Kronik, L.; Hodes, G.; Cahen, D. Are Mobilities in Hybrid Organic–Inorganic Halide Perovskites Actually "High"? *J. Phys. Chem. Lett.* **2015**, *6* (23), 4754–4757. https://doi.org/10.1021/acs.jpclett.5b02390.

(28) Zarazua, I.; Han, G.; Boix, P. P.; Mhaisalkar, S.; Fabregat-Santiago, F.; Mora-Seró, I.; Bisquert, J.; Garcia-Belmonte, G. Surface Recombination and Collection Efficiency in Perovskite Solar Cells from Impedance Analysis. *J. Phys. Chem. Lett.* **2016**, *7* (24), 5105–5113. https://doi.org/10.1021/acs.jpclett.6b02193.

Supporting Information

Radiative and non-Radiative Losses Analysis by In-situ Photoluminescence in Perovskite Solar Cell Current-Voltage Curves

Chris Dreessen,[1] Daniel Pérez-del-Rey,[1] Pablo P. Boix,[2*] Henk J. Bolink[1]

[1] Instituto de Ciencia Molecular, Universitat de València, c. J. Beltran 2, Paterna, Spain

[2] Institut de Ciència dels Materials, Universitat de València, c. J. Beltran 2, Paterna, Spain

* Corresponding author: pablo.p.boix@uv.es

Experimental methods

Photolithographically patterned ITO coated glass substrates were purchased from Naranjo Substrates. *N*4,*N*4,*N*4″,*N*4″-tetra([1,1′-biphenyl]-4-yl)-[1,1′:4′,1″-terphenyl]-4,4″-diamine (TaTm) were provided from Novaled GmbH. Fullerene (C_{60}) was purchased from sigma Aldrich. PbI_2 was purchased from Tokyo Chemical Industry CO (TCI), CH_3NH_3I (MAI), MoO_3 and BCP were purchased from Lumtec.

Device preparation

ITO prepatterned substrates were cleaned following a standard procedure where they are cleaned with soap, water, deionized water and isopropanol in a sonication bath, followed by a 20 min UV treatment. Then, the samples were transferred to a vacuum chamber integrated into a nitrogen-filled glovebox (H_2O and O_2 < 0.1 ppm) and evacuated to a pressure of 10^{-6} mbar. The chamber is equipped with an aluminium boat were MoO_3 is sublimed using a quartz crystal microbalance sensor (QCM) to control the evaporation rate and thickness. Afterwards, the MoO_3 layer was annealed at 100 ºC inside the glovebox for 10 minutes. The remaining layers were deposited in a second vacuum chamber equipped with six temperature-controlled evaporation sources (Creaphys) fitted with ceramic crucibles. The sample for the transmittance measurement was extracted after the evaporation of TaTm. The sources were directed upward with an angle of approximately 90° with respect to the bottom of the evaporator. The substrate holder to evaporation sources distance is approximately 20 cm. Three quartz crystal microbalance sensors are used: two monitoring the deposition rate of each evaporation source and a third one close to the substrate holder monitoring the total deposition rate.

For thickness calibration, we individually sublimed the charge transport materials. A calibration factor was obtained by comparing the thickness inferred from the QCM sensors with that measured with a mechanical profilometer (Ambios XP1). Then, the materials were sublimed at temperatures ranging from 160 ºC to >300 ºC, and the evaporation rate was controlled by separate QCM sensors obtaining precisely the deposited thickness. In general, the deposition rate for TaTm and C60 was 0.5 Å s^{-1} and 0.2-0.3 Å s^{-1} for the thinner layers (BCP). For the perovskite deposition MAI and PbI_2 were co-evaporated by measuring the deposition rate of each material in a different sensor and obtaining the total perovskite thickness in a third one, leading to 590 nm thick perovskite. Ag contacts were evaporated in the same vacuum chamber as the MoO_3.

Device characterization

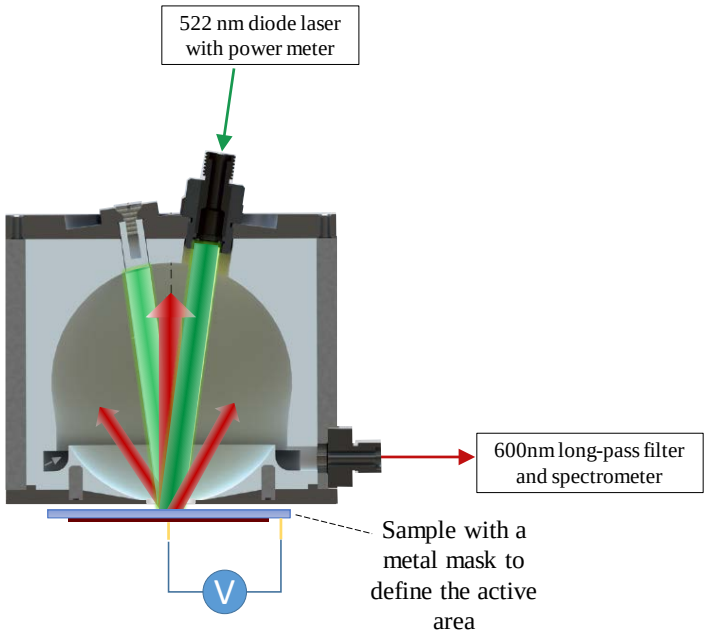

Figure S1: Scheme of the measurement setup.

For the simultaneous measurement of JV and PL the cell was placed on a self-made contacted holder, connected to a Keithley 2400 SourceMeter, and covered with a reflective shadow mask with 0.06 cm^2 aperture. An Avantes AvaSphere-50-REFL was placed onto the mask for light collection. The device was illuminated with a diode laser of integrated Optics, emitting at 522 nm. To control the laser power, 10% of the light were collected by an optical power meter via a fiber optic coupler with 90:10 splitting ratio. The light was collected behind a baffle to homogenize the light signal, send through an in-line 600nm long-pass filter and detected by a fiber optics based Avantes Avaspec2048 spectrometer. The system was calibrated to absolute photon numbers by a NIST traceable Avantes AvaLight-HAL-CAL-ISP50-MINI light sources which was placed in

front of the sample port. The PL and current (or voltage for a V_{OC} measurement) signal were recorded for 40s per voltage step, with a PL integrating time of 5s, to be able to observe time-dependent effects and to average for noise reduction. A forward scan from 0V to V_{OC} and a reverse scan from V_{OC} to -0.5V were acquired in 0.1V steps. Fast JV scans were obtained in a −0.2 to 1.2V voltage range, with 0.01V steps and integrating the signal for 20ms after a 10ms delay, corresponding to a speed of about 0.3V/s. In the analysis, the PL peaks were integrated from 1.47eV to 1.8eV and the result multiplied by the electric charge to calculate J_{rad}. $J_{extracted}$ was obtained by the mean of the current signal over time.

The JV curve under simulated AM1.5G illumination was recorded using a Keithley 2612A SourceMeter in a −0.2 and 1.2V voltage range, with 0.01V steps and integrating the signal for 20ms after a 10ms delay, corresponding to a speed of about 0.3V/s. The device was illuminated under a Wavelabs Sinus 70 LED solar simulator. The light intensity was calibrated before every measurement using a calibrated Si reference diode equipped with an infrared cutoff filter (KG-3, Schott). The layout used to test the solar cell has 4 equal areas (0.0651cm^2, defined as the overlap between the ITO and the top metal contact) and measured through a shadow mask with 0.06 cm^2 aperture.

Absorption spectra were collected using a fiber optics based Avantes Avaspec2048 spectrometer.

Reflection spectra were collected using an Avantes AvaSphere-50-REFL and a fiber optics based Avantes Avaspec2048 spectrometer.

<u>Estimation of the quasi-Fermi level splitting (QFLS) as an indication of correct absolute calibration</u>

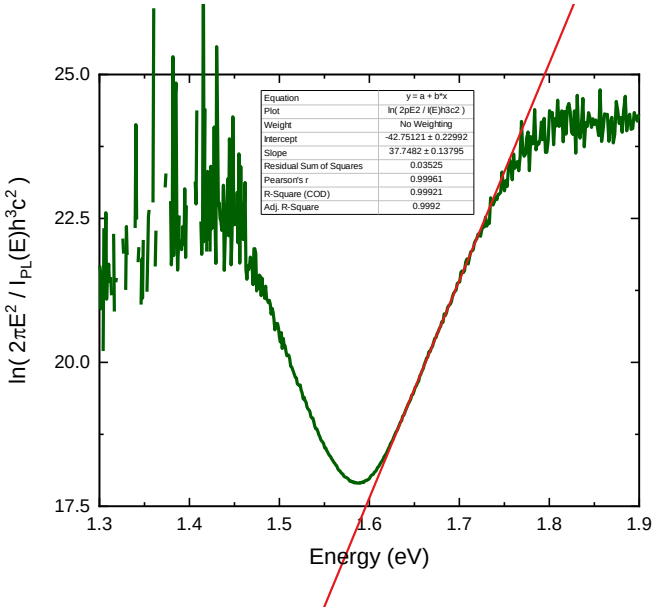

Figure S2: Plot of $\ln(2\pi E^2/I_{PL}(E)h^3c^2)$ with linear fit to estimate the QFLS.

Following previous reports[1], we use the Wien approximation of the generalized Planck's law,[2] which describes the spectral photon flux (I_{PL}) emitted by a body in non-equilibrium,

$$I_{PL}(E) = \frac{2\pi E^2 \alpha(E)}{h^3 c^2 \exp\left(\frac{E-\Delta\mu}{kT}\right)}. \quad \text{(S1)}$$

Here, E is the photon energy, α is the absorptivity, h the Planck constant, c the speed of light, k the Boltzmann constant, T the temperature and $\Delta\mu$ the QFLS. Assuming an absorptivity of 1 for energies above the bandgap, one can rearrange (S1) as a linear equation,

$$\ln\left(\frac{2\pi E^2}{I_{PL}(E)h^3c^2}\right) = \frac{E}{kT} - \frac{\Delta\mu}{kT}. \quad \text{(S2)}$$

The fit of our recorded spectrum at open-circuit conditions yields a temperature of T = 307 K and a QFLS of $\Delta\mu$ = 1.13eV which agrees excellently with the measured V_{OC} = 1.13V.

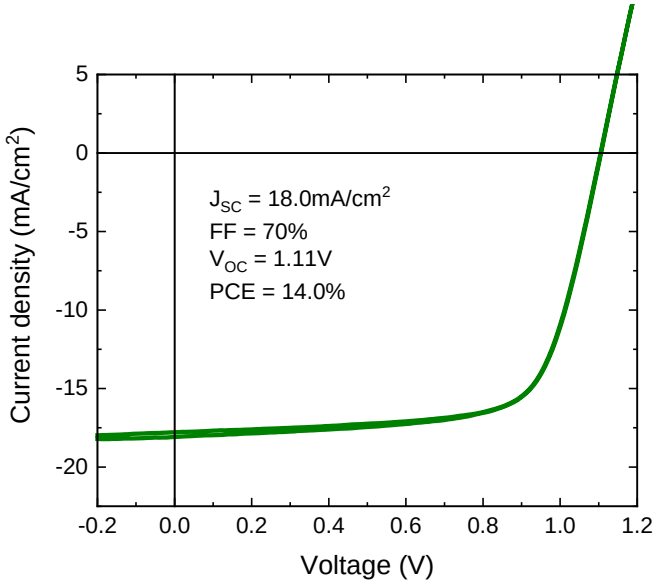

Figure S3: JV measurement under simulated AM1.5G illumination with parameters.

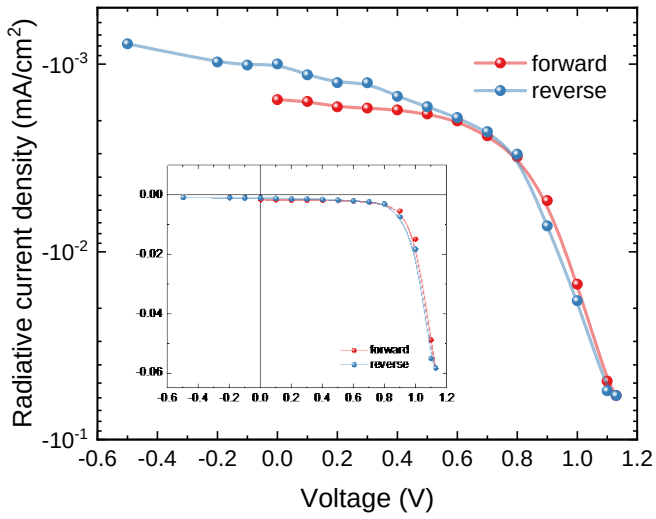

Figure S4: J_{rad} of the forward and reverse scan in logarithmic scale. Inset: The same in linear scale.

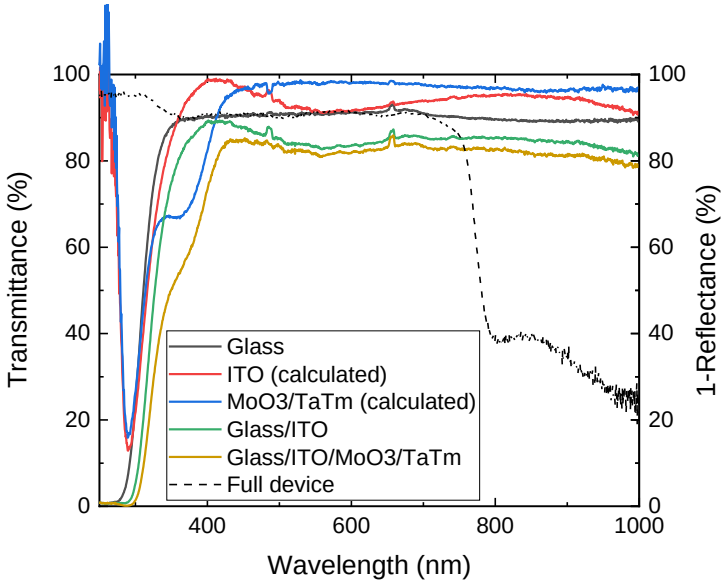

Figure S5: Transmittance of all the layers on top of the perovskite with reflectance of the full device.

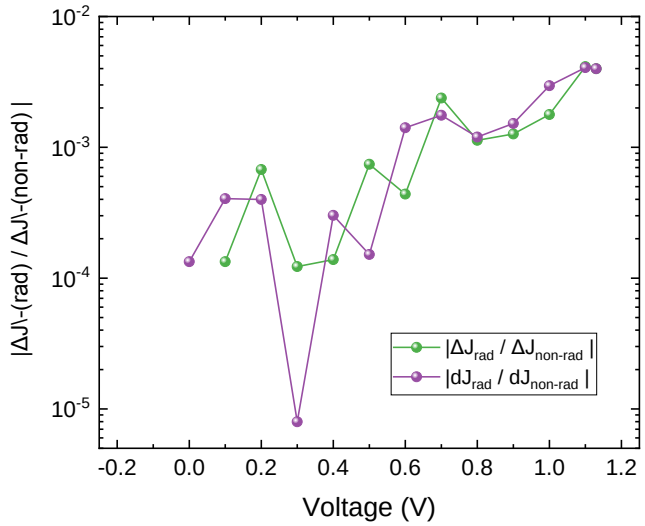

Figure S6: Comparison of Figure 3 and the derivation of the quantified $J_{non\text{-}rad}$ vs J_{rad} curve (both in the forward direction).

References

(1) Bauer, G. H.; Brüggemann, R.; Tardon, S.; Vignoli, S.; Kniese, R. Quasi-Fermi Level Splitting and Identification of Recombination Losses from Room Temperature Luminescence in Cu(In1-XGax)Se2thin Films versus Optical Band Gap. *Thin Solid Films* **2005**, *480–481*, 410–414. https://doi.org/10.1016/j.tsf.2004.11.061.

(2) P.Würfel. The Chemical Potential of Radiation. *J. Phys. C Solid State Phys.* **1982**, *15*, 3967–3985.